

RESEARCH PAPER

Co-Reduction Synthesis and Characterization of Yb³⁺-substituted ZnS Nanoparticles and Investigation of Catalytic Performance

Younes Hanifehpour

Department of chemistry, Sayyed Jamaledin Asadabadi University, Asadabad, Iran

ARTICLE INFO

Article History:

Received 17 July 2021

Accepted 04 October 2021

Published 15 October 2021

Keywords:

Ytterbium

Photocatalysis

Nanoparticles

ZnS

Degradation

ABSTRACT

Pure and Yb³⁺-doped ZnS (Yb_xZn_{1-x}S) nanoparticles were prepared in this research via hydrothermal route at 160 °C and for 12 h. The obtained products were characterized by scanning electron microscopy (SEM), X-ray photoelectron spectroscopy (XPS), transmission electron microscopy (TEM), and X-ray powder diffraction (XRPD). Analyses of XRPD data showed that the particles were perfectly crystallized and assigned to the cubic structure of zinc sulfide. TEM and SEM images indicated that the sizes of particles were in the range of 10-80nm. The photocatalytic performance of Yb³⁺-doped ZnS nanoparticles was assessed in an aqueous solution by observing the decolorization of Tartrazine (Yellow 5) in the process of visible-light radiation. The degradation percentage of Yb_{0.06}Zn_{0.94}S and bare ZnS were 92.15 and 22.10%, respectively, after 100 min of treatment. Six percent Yb³⁺-doped ZnS nanoparticles demonstrated the highest removal efficiency among various values of the dopant agent. It was noticed that the existence of inorganic ions such as C₂O₄²⁻, I⁻, and other radical scavengers including benzoquinone and butanol decreased the decolorization efficiency.

How to cite this article

Hanifehpour Y. Co-Reduction Synthesis and Characterization of Yb³⁺-substituted ZnS Nanoparticles and Investigation of Catalytic Performance. *Nanochem Res*, 2021; 6(2):202-212. DOI: 10.22036/ncr.2021.02.007

INTRODUCTION

Recently, nano-crystalline semiconductors have been chiefly investigated as the most favorable photocatalyst for environmental remediation such as water refinement, air purification, hazardous waste remediation, and heavy metals degradation due to their non-secondary pollution and high functionality [1-5]. Due to the unpleasant influence of organic molecules on human safety, various treatment processes have been employed for treating colored effluents including biological treatment, flocculation/coagulation, chemical oxidation, advanced oxidation processes, membrane filtration, electrochemical oxidation, adsorption, and ion exchange [6-9]. Research of doping agents or impurity effects on the physical characteristics of semiconductors exist for both applied and basic studies. Rare-earth cations

containing unoccupied 4f and empty 5d orbitals are frequently utilized as photo-catalysts or enhanced catalysis. In addition, doping with lanthanide ions with 4f electron configurations could exceptionally boost the isolation rate of photo-induced charge carriers in photocatalysts and significantly promote the catalytic ability [10-15].

Zinc sulfide is an essential II-VI semiconductor compound with a wide direct band-gap of E_g = 3.68 eV (bulk) [16]. ZnS has been examined owing to its vast potentials as catalysts and phosphors. ZnS is also appropriate for various technologies such as solar cells, electro-luminescent devices, and many other optoelectronic devices due to its stability in virtually all environments, high resistance to thermal shock, and extra-low bulk losses. Further, Zinc sulfide is a potent and promising catalyst for the photocatalytic removal of organic dyes as reported

* Corresponding Author Email: younes.hanifehpour@gmail.com

by several researchers [17-20]. In this study, a facile hydrothermal process was used for preparing undoped and Yb³⁺-substituted ZnS (Yb_xZn_{1-x}S) particles. The photocatalytic performance of such particles towards the decolorization of Tartrazine (as a model organic dye) with visible-light radiation was evaluated. Table 1 provides the characteristics of Yellow 5. Considering the literature, there is no previous report related to the use of ZnS and Yb_xZn_{1-x}S particles for the elimination of Tartrazine (Yellow 5). Furthermore, this study aims to assess the influence of inorganic ions on the degradation percentage of Yellow 5.

MATERIALS AND METHODS

Chemicals

All chemicals utilized in this research were of analytical grade and used without further purification. NaOH, N₂H₄·H₂O (99%), ZnSO₄·6H₂O (99.5%) and S (99%) were obtained from Merck; Yb(NO₃)₃·5H₂O and ethanol (99%) were acquired from Aldrich, and Tartrazine from Zhejiang Yide Chemical Co. (China).

Synthesis of Yb³⁺-doped ZnS compounds

Yb³⁺-doped ZnS particles with different Yb³⁺ contents (0-6% mol) were synthesized employing hydrazine hydrate (N₂H₄·H₂O) as the reducing factor using the hydrothermal method. In a normal preparation, appropriate molar ratios of Yb(NO₃)₃·5H₂O, 2 mmol S, 1 mmol NaOH and ZnSO₄·6H₂O were first dissolved in 25 mL distilled water. Hydrazine hydrate (N₂H₄·H₂O) was then added drop-wise to the above solution under middle-speed stirring. After constant stirring, the

resulting solution was moved into a 50 ml Teflon-lined stainless-steel, placed in an oven at 160°C for 12h, and subsequently, the autoclave was cooled naturally to room temperature. As-obtained Yb_xZn_{1-x}S particles were collected and washed with absolute ethanol and distilled water several times for eliminating residual impurities, and then vacuum-dried at 70 °C for 2 h. As a result, the final yellow–white powders were obtained.

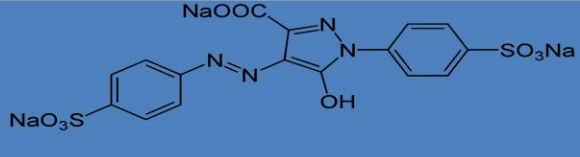
Characterization Methods

The XRPD characterization was employed for determining the crystal phase composition of samples at room temperature by using a D8 Advance diffractometer (Bruker, Karlsruhe, Germany) with high-intensity monochromatic Cu K α radiation ($\lambda=1.5406 \text{ \AA}$), accelerating voltage of 40 kV, and emission current of 30 mA. The surface state and the morphology were observed via an electron microscope (SEM, S-4200, Hitachi, Tokyo, Japan), and the chemical state of the constituent elements as well as chemical identification were analyzed by using X-ray photoelectron spectroscopy, XPS (K-ALPHA, UK), and Thermo Scientific spectrophotometer. Cell parameters were measured through Celref program based on PXRD patterns, and reflections were determined and fitted by applying a profile-fitting procedure with the Winxpow program. The reflections observed in $2\theta= 10\text{--}80^\circ$ were employed for identifying the lattice parameter.

Photo-catalytic investigation

The catalytic performance of bare and Yb³⁺-doped ZnS nanoparticles were assessed in an

Table 1. The characteristics of Yellow 5

Chemical structure	
Color index name	Yellow 5
Other Names	Tartrazine
Molecular formula	C ₁₆ H ₉ N ₄ Na ₃ O ₉ S ₂
Color index number	C.I.19140
λ_{max} (nm)	428
M _w (g/mol)	534.36

aqueous solution under visible light by monitoring the degradation of Yellow 5. In a usual method, 0.1 g of the photocatalyst material was added to 100 ml Yellow 5 solution with a starting concentration of 5 mg/l. The suspended photocatalyst and Yellow 5 were magnetically stirred in a quartz photoreactor in the dark for 100 min to form an adsorption/desorption equilibrium of the dye. Then, a 40 W visible-light lamp was used for irradiating the solution. The degradation percentage (DE (%)) was stated as the ratio of decolorized dye concentration to that of the initial one multiplied by 100. During the photocatalytic process, 5 ml of the suspension was sampled at a desired time and after centrifugation; the removal of color was assessed through UV-Vis spectrophotometer by determining the absorbance of the solution at $\lambda_{\max} = 428 \text{ nm}$.

RESULTS AND DISCUSSION

Physical properties and characteristics of as-prepared materials

Fig. 1 displays the XRPD patterns of the pure and Yb³⁺-substituted ZnS samples. The observed

diffraction peaks of the as-prepared compounds can be attributed to the pure, typical, and well-crystallized cubic ZnS (JCPDS No. 05-0566)[21]. No peaks showing impurities were observed, confirming that the hydrothermal route applied in this study was successful in preparing the desired samples. Additionally, the sharp peaks in the XRPD patterns of the prepared samples indicate that the obtained products were high crystalline. Behind doping values of $x = 0.06$ for Yb³⁺, extra undisclosed phases were observed. There was a slight shift to the lower diffraction angles in the 6 % Yb³⁺-doped ZnS pattern. This result can be related to the expansion of ZnS lattice due to the presence of Yb³⁺ ions which have larger radii (0.99 Å) compared with Zn²⁺ ions (0.74 Å). Moreover, this shift to lower angles confirms the successful doping of Yb³⁺ into the Zn²⁺ lattice.

The cell parameters of the as-obtained samples were calculated by XRPD patterns. With increasing dopant content (x), a parameter for Yb³⁺ increased (Figure 2). The shift for lattice constants can be related to the effective ionic radii of the Ln³⁺ ions, which led to larger lattice parameters for Yb³⁺ doped samples.

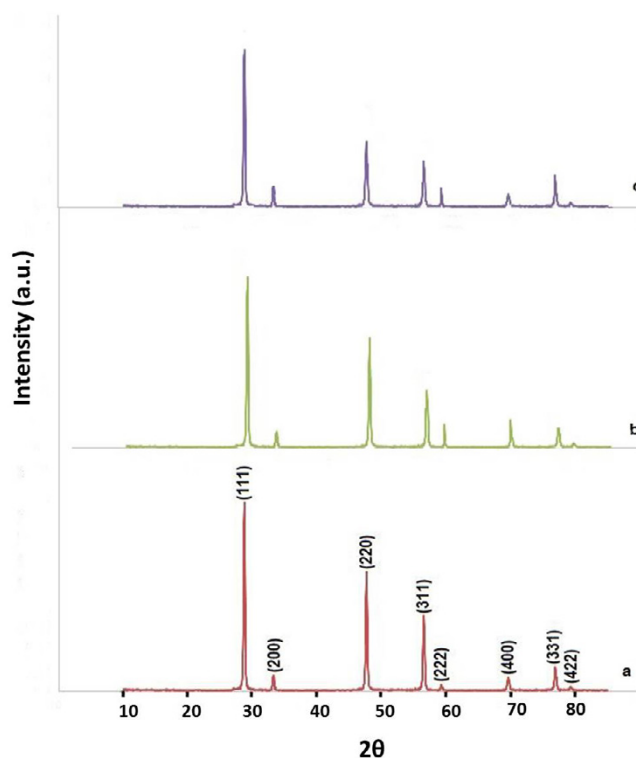


Fig. 1. X-ray powder diffraction pattern of Yb_xZn_{1-x}S ((a) $x = 0.0$, (b) $x = 0.04$, (c) $x = 0.06$) synthesized at 160 °C and 12 h

XPS analysis was utilized to examine the valence state and the chemical composition of Yb in the 6% Yb³⁺-doped ZnS particles (Fig. 3). The binding energy for the Zn2p region of Yb³⁺-doped ZnS is shown in Fig. 3a. The Zn 2p_{1/2} and 2p_{3/2} peaks were detected at around 1047.2 and 1022.4 eV which can be attributed to the Zn element in zinc sulfide,

validating the oxidation state of 2 for Zn in the 6% Yb³⁺-doped ZnS sample [22, 23]. The S2p curve of ZnS manifested a strong peak at around 162.9 eV, which is ascribed to the coordination of Sulfur and Zn atoms (Zn–S–Zn) in the structure of ZnS (Fig. 3b) [24]. As shown in Fig. 3c, two peaks centered at 186.2 and 200.18 eV can be related to the Yb 4d_{5/2}

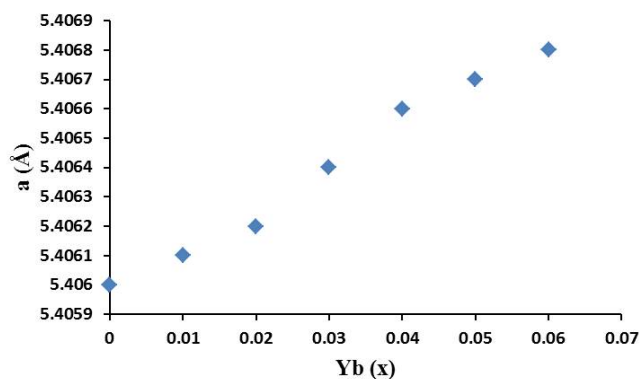


Fig. 2. The lattice constant of Yb_xZn_{1-x}S (x = 0 to 0.06) dependent upon Yb³⁺ doping on Zn²⁺ sites.

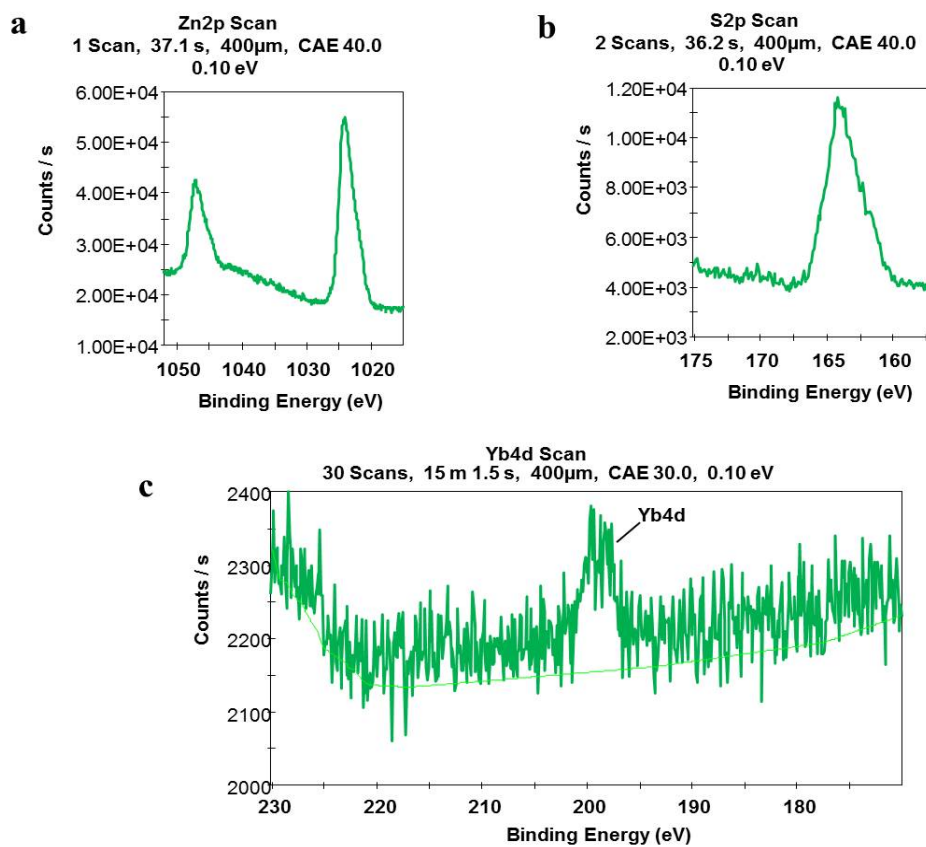


Fig. 3. XPS of 6% Yb³⁺-doped ZnS.

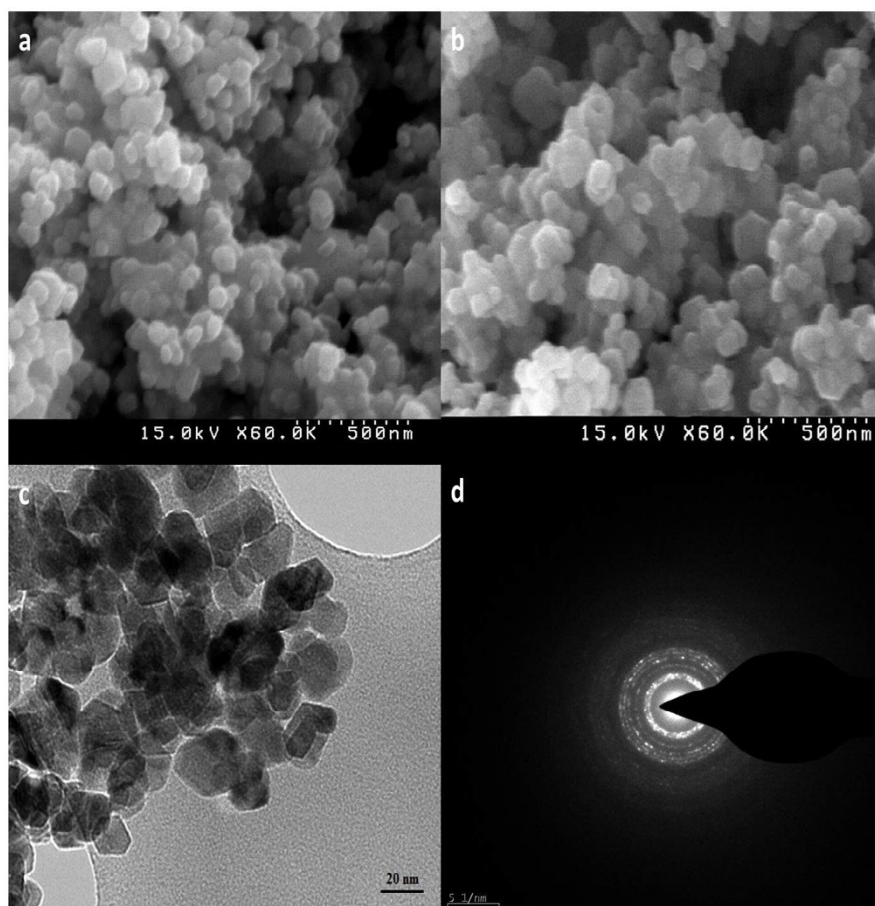


Fig. 4. SEM images of the (a) ZnS and (b) $Zn_{0.94}Yb_{0.06}S$ and (c) TEM image of $Zn_{0.94}Yb_{0.06}S$ and (d) SAED pattern of $Zn_{0.94}Yb_{0.06}S$.

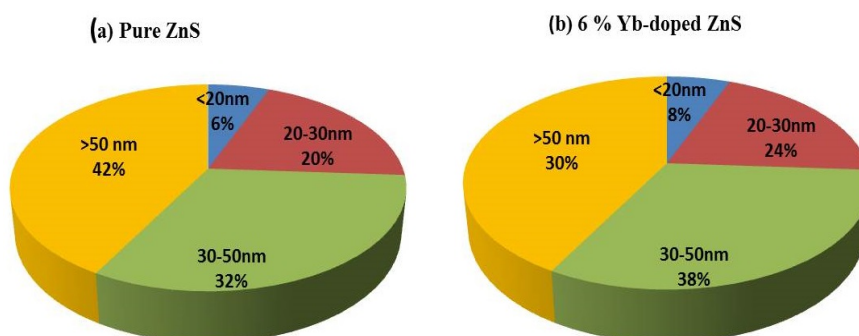


Fig. 5. Size distribution of ZnS (a) and 6% Yb^{3+} -doped ZnS (b) nanomaterials

and $Yb\ 4d_{3/2}$, respectively [25].

TEM and SEM analyses were conducted for investigating the morphologies of the products. In Fig. 4a and b, spherical and uniform particles of about 10–80 nm in diameter with a little agglomeration can be observed. Through

incorporating Yb^{3+} ions into the lattice of ZnS, the size and surface morphology of the sample had no clear changes. Fig. 4c and d show TEM image and SAED pattern of the 6% Yb^{3+} sample which validates the SEM output and good crystallinity of materials.

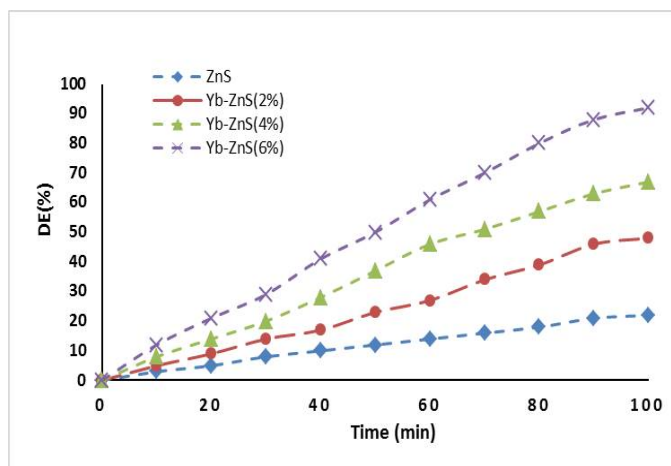


Fig. 6. The effect of Yb^{3+} dopant content on the decolorization of 10 mg/L Yellow 5 (catalyst loading 1.0 g/L)

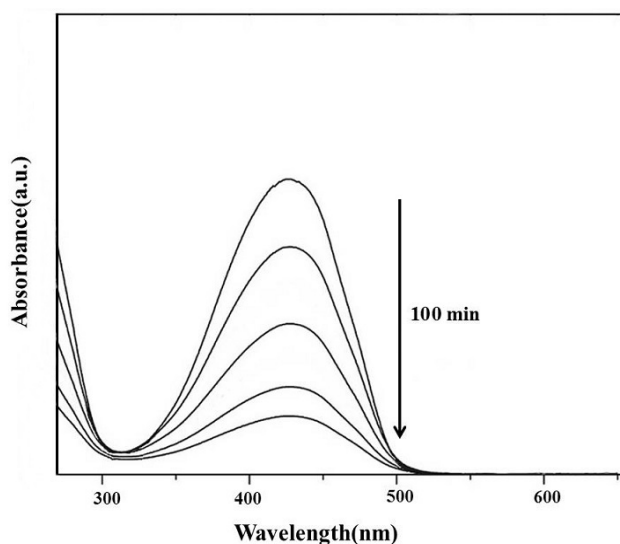


Fig. 7. Adsorption and degradation of Yellow 5 under visible light irradiation using $\text{Yb}_{0.06}\text{Zn}_{0.94}\text{S}$ nanoparticles

Size distribution for Yb^{3+} -doped ZnS particles was attained to be in the range of 10–80 nm, which is smaller than that of pure ZnS (Fig. 5).

Effect of operating conditions on the photocatalysis of Yellow 5

Effect of Yb^{3+} content of $\text{Yb}_x\text{Zn}_{1-x}\text{S}$ nanoparticles

The degradation process of Tartrazine (Yellow 5) was examined under visible light irradiation by $\text{Yb}_x\text{Zn}_{1-x}\text{S}$ with various mole fractions ($x = 0.00, 0.01, 0.02, 0.04, 0.06$) in order to explore the perfect conditions of photocatalytic performance. Fig. 6 demonstrates the degradation percentage of Yellow 5 over divergent Yb^{3+} -doped ZnS catalysts

during 100 min of the reaction. As indicated in Fig. 5, the nanomaterials doped with proper content of Yb^{3+} ion enhanced the photocatalytic performance much more than bare ZnS did. Specifically, the sample with the Yb^{3+} molar ratio of 0.06 manifested the best catalytic activity. The reason for high photocatalytic activity of $\text{Yb}_{0.06}\text{Zn}_{0.94}\text{S}$ can be explained in the following way. Normally, rare-earth cations can perform either as a recombination center or as a mediator of interfacial charge in the crystalline structure of the photocatalyst [26, 27]. Therefore, based on the dopant value, the doped ZnS performance or efficiency is changeable. At low mole content of dopant, Yb^{3+} ions can retard

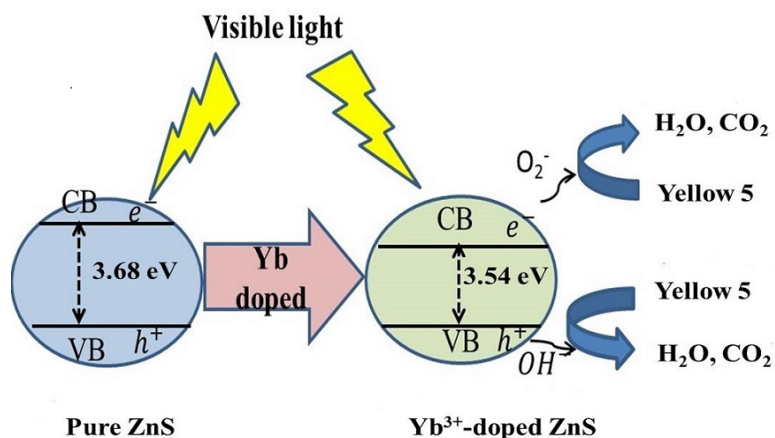


Fig. 8. The schematic illustration of photocatalysis

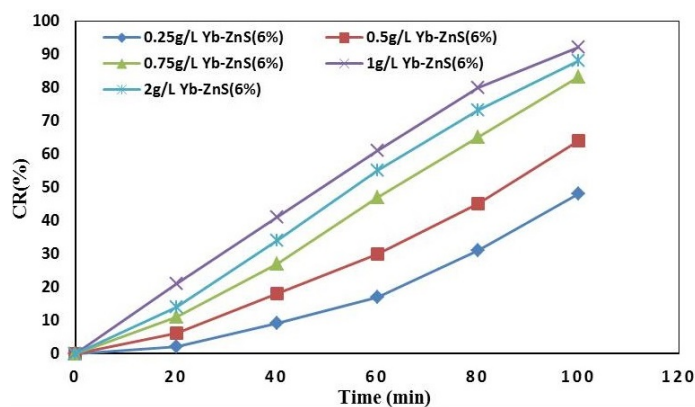


Fig. 9. Influence of catalyst loading on the decolorization of 10 mg/L Yellow 5 by the $\text{Yb}_{0.06}\text{Zn}_{0.94}\text{S}$

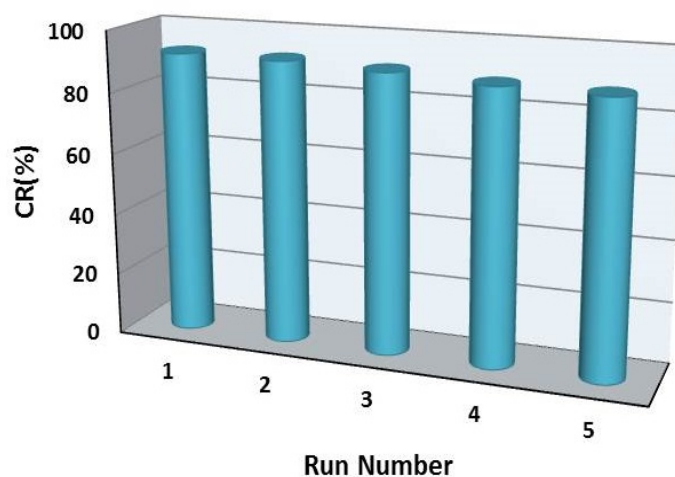


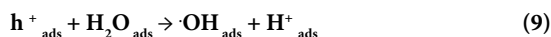
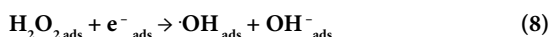
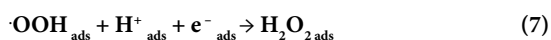
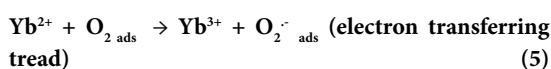
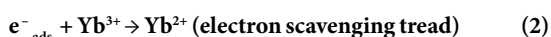
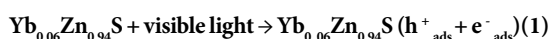
Fig. 10. Reusability results of $\text{Yb}_{0.04}\text{Zn}_{0.96}\text{S}$ in photocatalytic decolorization of 10 mg/L of Yellow 5 in the presence of 1.0 g/L of $\text{Yb}_{0.06}\text{Zn}_{0.94}\text{S}$ and irradiation time of 100 min

electron/hole recombination rate by capturing photoinduced electrons, and, consequently, promoting the interfacial charge transfer for Yellow 5 degradation [28]. However, when the mole ratio of the doping agent is greater than the maximum value, the recombination rate may increase by decreasing the distance between the trapping sites in ZnS structure, leading to a reduction in the catalytic activity. Thus, the best content of Yb³⁺ is substantial in isolating the photo-induced electron/hole pairs and boosting the lifetime of charge carriers.

Photo-catalytic decolorization mechanism of Yellow 5 on Yb_{0.06}Zn_{0.94}S

In order to properly explain the photocatalytic performance of the Yb_{0.06}Zn_{0.94}S samples and assess the realizable mechanism of reaction, the UV-Vis absorption spectra of Yellow 5 at different irradiation times for the photocatalytic process are shown in Fig. 7. The decreasing concentration of Yellow 5 during the catalytic procedure is utilized to evaluate the potential of the catalyst.

Here, the doping Yb³⁺ acts as an electron predator on the surface of ZnS, repressing the recombination of electron-hole pairs and increasing their lifetime; therefore, the photo-catalytic activity of the catalyst is elevated. The realizable mechanism for the elevated photocatalysis of Sm_{0.04}Zn_{0.96}S is suggested as follow. The electrons (e⁻) are excited from the valence band to the conduction band of ZnS through visible light irradiation, and the holes (h⁺) are generated. Yb³⁺ content in ZnS can efficiently scavenge the electrons and hinder their recombination with h⁺ due to the existence of partially filled 4f-orbital [29, 30]. The decolorization mechanism for the Yb_{0.06}Zn_{0.94}S is provided in Eqs 1-10.



The schematic illustration of the catalytic activity of as-prepared nanoparticles is presented in Fig. 8.

The outcome of catalyst concentration and reusability

The starting rate of photocatalytic degradation process relies on the catalyst concentration [31]. The effect of catalyst loading on the elimination percentage of Yellow 5 can be seen in Fig. 9. The color removal ratios were 47.85, 62.48, 81.29, 92.15 and 88.45 % at the concentrations of 0.25, 0.5, 0.75, 1.0, and 2 g/L, respectively. The DE% increased from 0.25 to 1.0 g/L, and then declined. This could be explained by the aggregation of catalyst beyond 1.0 g/L which resulted in reducing the number of active sites.

Reusability is one of the most substantial parts for a catalyst. Fig.10 shows the reusability assays of Yb_{0.06}Zn_{0.94}S catalyst in the degradation of Yellow 5, during the 5 round tests under the perfect condition of 100 min for irradiation time, 10 mg/L of tartrazine, 1.0 g/L of Yb_{0.06}Zn_{0.94}S photo catalyst. Following each degradation test, the catalyst was washed with distilled water, dried at 70 °C for 2h, and utilized in the next run. As shown in Fig. 10, Yb_{0.06}Zn_{0.94}S manifested outstanding chemical firmness without any significant decomposition or photo-corrosion during the 5 rounds of the catalytic reaction, suggesting that it is a superior catalyst for empirical applications.

Effect of Initial Yellow 5 concentrations

Various initial dye concentrations in the range of 10 to 30 mg/L were used in this research. According to Fig. 11, DE percentage reduced from 92.15 to 59.81% for the initial concentration of 10 to 30 mg/L. Filling the energetic sites on the catalyst surface by pollutant molecules at high concentrations results in an astounding decrease in the degradation effectiveness. Preventing the diffusion of light to the catalyst surface can lead to unsatisfactory performance at a dense concentration of dye solution.

The role of radical scavengers on the photocatalytic performance

To evaluate the mechanism of decolorization process and to find the chief oxidative species,

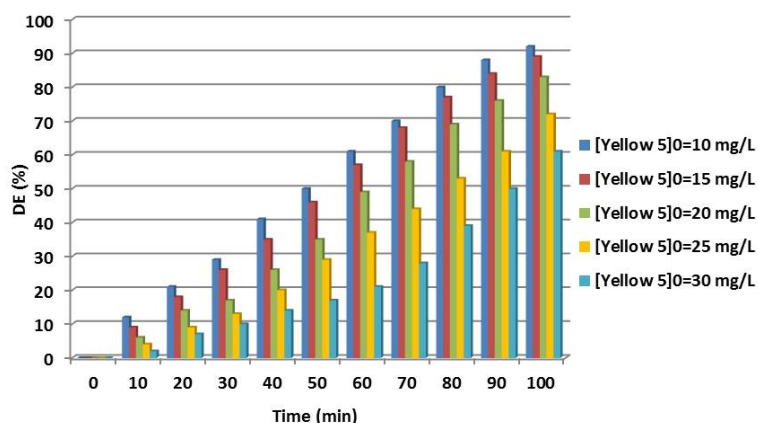
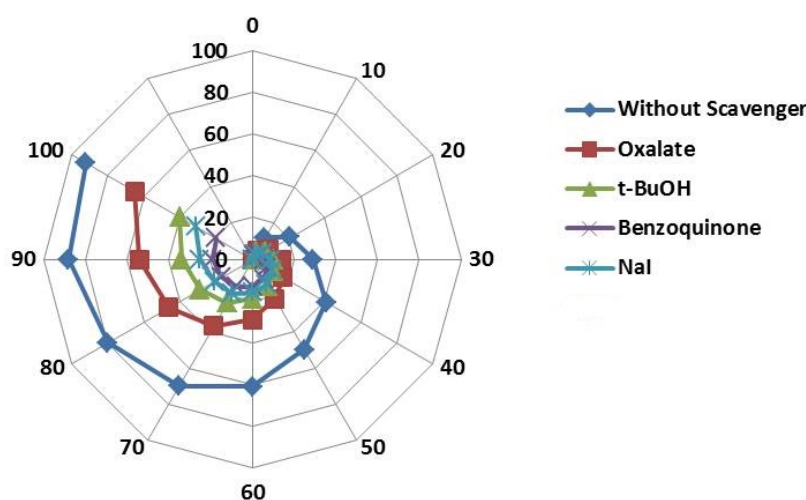


Fig. 11. Yellow 5 concentration influence on degradation efficiency

Fig. 12. Effects of adding I^- , benzoquinone, butanol, and oxalate ions on the decolorization of 10 mg/L Yellow 5 ($Yb_{0.06}Zn_{0.94}S$ loading 1.0 g/L)

assays were conducted in the presence of proper scavengers of active species. As indicated by Fig. 12, by separately adding oxalate (a scavenger of h^+_{VB}), t-BuOH (a scavenger of hydroxyl radicals), and I^- (scavenger of hole), the decolorization percentage reduces to 65.39%, 52%, and 31.67 %, respectively. In the case of benzoquinone (BQ) (a scavenger of superoxide radicals), the dye degradation was hindered extraordinarily. These results demonstrate that superoxide radicals and the h^+_{VB} were the principal oxidative species in decomposing dye structure. Moreover, the hydroxyl radicals influence the decolorization.

CONCLUSION

In this research, pure and Yb^{3+} -doped ZnS were obtained by a simple hydrothermal approach and

employed as a photocatalyst under visible light irradiation for removing Yellow 5. XRD analysis displayed well crystalline cubic structure of ZnS, and the substitution of Yb^{3+} ions into the ZnS lattice was validated by the XPS analysis. In addition, the surface morphology and size of the samples had no obvious changes after incorporating Yb^{3+} into the lattice of ZnS. The results indicated that the decolorization efficiency of Yb^{3+} -doped ZnS was higher than that of pure ZnS, and the degradation efficiency was significantly affected by the content of Yb dopant in ZnS. The promoted decolorization efficiency was found in the presence of 6% Yb^{3+} -doped ZnS particles. The color removal percentages of $Yb_{0.06}Zn_{0.94}S$ and undoped ZnS were 92.15 and 22.37% after 100 min of treatment, respectively. Benzoquinone led to the highest negative effect

on the photocatalysis of Yellow 5. Generally, the application of Yb³⁺-doped ZnS particles can be a promising and effective approach for the elimination of colored effluents.

ACKNOWLEDGMENT

This work is funded by Sayyed Jamaledin Asadabadi University Research Grant.

REFERENCES

- [1] Khataee A, Darvishi Cheshmeh Soltani R, Hanifehpour Y, Safarpour M, Gholipour Ranjbar H, Joo SW. Synthesis and Characterization of Dysprosium-Doped ZnO Nanoparticles for Photocatalysis of a Textile Dye under Visible Light Irradiation. *Industrial & Engineering Chemistry Research*. 2014;53(5):1924-32.
- [2] Tryk DA, Fujishima A, Honda K. Recent topics in photoelectrochemistry: achievements and future prospects. *Electrochimica Acta*. 2000;45(15):2363-76.
- [3] Forghani B, Fazaeli R, Aliyan H. Sunlight Assisted Photodecolorization of Methylene Blue Catalyzed by H3PW12O40 Grafted on APTMS-Graphene Oxide. *Nanochemistry Research*. 2020;5(2):197-210.
- [4] Taghavi Fardood S, Moradnia F, Ghalaichi AH, Danesh Pajouh S, Heidari M. Facile green synthesis and characterization of zinc oxide nanoparticles using tragacanth gel: investigation of their photocatalytic performance for dye degradation under visible light irradiation. *Nanochemistry Research*. 2020;5(1):69-76.
- [5] Taghavi Fardood S, Moradnia F, Moradi S, Foroootan R, Yekke Zare F, Heidari M. Eco-friendly synthesis and characterization of α -Fe₂O₃ nanoparticles and study of their photocatalytic activity for degradation of Congo red dye. *Nanochemistry Research*. 2019;4(2):140-7.
- [6] Darvishi Cheshmeh Soltani R, Khataee AR, Safari M, Joo SW. Preparation of bio-silica/chitosan nanocomposite for adsorption of a textile dye in aqueous solutions. *International Biodeterioration & Biodegradation*. 2013;85:383-91.
- [7] Ghicov A, Schmuki P. Self-ordering electrochemistry: a review on growth and functionality of TiO₂ nanotubes and other self-aligned MOx structures. *Chemical Communications*. 2009(20):2791.
- [8] Aazam ES, Mohamed RM. Environmental remediation of Direct Blue dye solutions by photocatalytic oxidation with cuprous oxide. *Journal of Alloys and Compounds*. 2013;577:550-5.
- [9] Primo A, Corma A, García H. Titania supported gold nanoparticles as photocatalyst. *Phys Chem Chem Phys*. 2011;13(3):886-910.
- [10] Liqiang J, Xiaojun S, Baifu X, Baiqi W, Weimin C, Honggang F. The preparation and characterization of La doped TiO₂ nanoparticles and their photocatalytic activity. *Journal of Solid State Chemistry*. 2004;177(10):3375-82.
- [11] Alemi A, Hanifehpour Y, Joo SW, Min B-K. Synthesis of novel Ln_xSb_{2-x}Se₃ (Ln: Lu³⁺, Ho³⁺, Nd³⁺) nanomaterials via co-reduction method and investigation of their physical properties. *Colloids and Surfaces A: Physicochemical and Engineering Aspects*. 2011;390(1-3):142-8.
- [12] Hanifehpour Y, Soltani B, Amani-Ghadim AR, Hedayati B, Khomami B, Joo SW. Praseodymium-doped ZnS nanomaterials: Hydrothermal synthesis and characterization with enhanced visible light photocatalytic activity. *Journal of Industrial and Engineering Chemistry*. 2016;34:41-50.
- [13] Hanifehpour Y, Woo Joo S. Synthesis, characterization and sonophotocatalytic degradation of an azo dye on Europium doped cadmium selenide nanoparticles. *Nanochemistry Research*. 2018;3(2):178-88.
- [14] Hanifehpour Y. Modified Y₂O₃-coated biosilica with Dysprosium nanomaterials: synthesis, characterization, optical study with enhanced catalytic activity. *Nanochemistry Research*. 2021;6(1):122-34.
- [15] Alemi A, Hanifehpour Y, Woo Joo S, Khandar A, Morsali A, Min B-K. Co-reduction synthesis of new Ln_xSb_{2-x}Se₃ (Ln: Nd³⁺, Lu³⁺, Ho³⁺) nanomaterials and investigation of their physical properties. *Physica B: Condensed Matter*. 2011;406(14):2801-6.
- [16] Sooklal K, Cullum BS, Angel SM, Murphy CJ. Photophysical Properties of ZnS Nanoclusters with Spatially Localized Mn²⁺. *The Journal of Physical Chemistry*. 1996;100(11):4551-5.
- [17] Zhu Y-C, Bando Y, Xue D-F. Spontaneous growth and luminescence of zinc sulfide nanobelts. *Applied Physics Letters*. 2003;82(11):1769-71.
- [18] Dong F, Guo Y, Zhang J, Li Y, Yang L, Fang Q, et al. Size-controllable hydrothermal synthesis of ZnS nanospheres and the application in photocatalytic degradation of organic dyes. *Materials Letters*. 2013;97:59-63.
- [19] Pathak CS, Mishra DD, Agarwala V, Mandal MK. Optical properties of ZnS nanoparticles produced by mechanochemical method. *Ceramics International*. 2012;38(8):6191-5.
- [20] El-Kemary M, El-Shamy H. Fluorescence modulation and photodegradation characteristics of safranin O dye in the presence of ZnS nanoparticles. *Journal of Photochemistry and Photobiology A: Chemistry*. 2009;205(2-3):151-5.
- [21] Xu JF, Ji W, Lin JY, Tang SH, Du YW. Preparation of ZnS nanoparticles by ultrasonic radiation method. *Applied Physics A: Materials Science & Processing*. 1998;66(6):639-41.
- [22] Ngom BD, Chaker M, Manyala N, Lo B, Maaza M, Beye AC. Temperature-dependent growth mode of W-doped ZnO nanostructures. *Applied Surface Science*. 2011;257(14):6226-32.
- [23] Jia T, Wang W, Long F, Fu Z, Wang H, Zhang Q. Fabrication, characterization and photocatalytic activity of La-doped ZnO nanowires. *Journal of Alloys and Compounds*. 2009;484(1-2):410-5.
- [24] Durn JDG, Guindo MC, Delgado AV. Electrophoretic Properties of Colloidal Dispersions of Monodisperse Zinc Sulfide: Effects of Potential-Determining Ions and Surface Oxidation. *Journal of Colloid and Interface Science*. 1995;173(2):436-42.
- [25] Singh BP, Parchur AK, Ningthoujam RS, Ramakrishna PV, Singh S, Singh P, et al. Enhanced up-conversion and temperature-sensing behaviour of Er³⁺ and Yb³⁺ co-doped Y₂Ti₂O₇ by incorporation of Li⁺ ions. *Phys Chem Chem Phys*. 2014;16(41):22665-76.
- [26] Khataee A, Khataee A, Fathinia M, Hanifehpour Y, Joo SW. Kinetics and Mechanism of Enhanced Photocatalytic Activity under Visible Light Using Synthesized Pr_xCd_{1-x}Se Nanoparticles. *Industrial & Engineering Chemistry Research*. 2013;52(37):13357-69.
- [27] Hamnabard N, Hanifehpour Y, Khomami B, Woo Joo S.

- Synthesis, characterization and photocatalytic performance of Yb-doped CdTe nanoparticles. *Materials Letters*. 2015;145:253-7.
- [28] Sin J-C, Lam S-M, Lee K-T, Mohamed AR. Photocatalytic performance of novel samarium-doped spherical-like ZnO hierarchical nanostructures under visible light irradiation for 2,4-dichlorophenol degradation. *Journal of Colloid and Interface Science*. 2013;401:40-9.
- [29] Kim M-J, Choi YI, Joo SW, Kang M, Sohn Y. Synthesis of Er and Yb-doped cubic and hexagonal phase ZnSe nano-assembled microspheres and their photocatalytic activities. *Ceramics International*. 2014;40(10):16051-9.
- [30] Khataee AR, Hanifehpour Y, Safarpour M, Hosseini M, Joo SW. Synthesis and Characterization of $\text{Er}_x\text{Zn}_{1-x}\text{Se}$ Nanoparticles: A Novel Visible Light Responsive Photocatalyst. *Science of Advanced Materials*. 2013;5(8):1074-82.
- [31] Ghosh T, Ullah K, Nikam V, Park C-Y, Meng Z-D, Oh W-C. The characteristic study and sonocatalytic performance of CdSe-graphene as catalyst in the degradation of azo dyes in aqueous solution under dark conditions. *Ultrasonics Sonochemistry*. 2013;20(2):768-76.